Available online at www.sciencedirect.com
ScienceDirect
Journal of the European Ceramic Society 27 (2007) 3459–3467
www.elsevier.com/locate/jeurceramsoc

Surface ionics: A brief review

V.V. Belousov

Department of Functional Ceramics, Institute of Ceramics, Russian Academy of Sciences, 48 Ozernaya Str., 119361 Moscow, Russia

Received 1 September 2006; received in revised form 3 January 2007; accepted 27 January 2007
Available online 2 April 2007

Abstract

Experimental and theoretical data on the surface electrical and mass transport processes in ionic materials (ceramics, composites, and nanostructures) are summarized and discussed. Important role of interfaces in the transport processes is exhibited. Influence of surface phase transitions on transport properties of ionic materials is considered.

Keywords: Interfaces; Ionic conductivity; Diffusion; Interface phase transitions

1. Introduction

Surface is one from the fundamental defects of the crystal structure. Rupture of the chemical bonds at the surface leads to the change of coordination sphere of atoms. The disordered structure of surface cannot by jump to pass into regular structure of the crystal bulk and there is any transitional zone.

According to the principle of global electrical neutrality, accumulation of electronic or ionic charge at the surface of ionic materials induces the formation of space charge region.[1,2] Ionic conduction in the space charge region can differ from that in the crystal bulk.[3] When crystal size approaches to the space charge width, the surface and bulk properties are related (classical size effect).[1,4]

Surface phase transitions can substantially influence ionic conduction of materials.[5]

Numerous ionic conductors[6] have a high specific surface. Interest to study surface ionic conduction was initiated by Liang's publication[7] reporting an enhancement of Li^+ ion conductivity by a factor of almost 50 for LiI/Al_2O_3 composite in comparison with pure LiI. During the last decades there has been a growing interest in different aspects of surface ionics stimulated by intensive development of micro- and nanoionics technology.[8] Significant contribution in development of the surface ionics was made by J.B. Wagner[9] and especially by J. Maier.[2,3]

The aim of this article is to summarize and discuss some important experimental and theoretical data in field of surface ionics. In order to keep this article within limits, for more details the reader is referred to the original publications.

2. Ionic conduction

Wagner's equation[10] describes a flux of ions, J_i, in material under electrochemical field:

$$J_i = \left(\frac{\sigma_i}{q_i^2}\right) \nabla \eta_i \tag{1}$$

where q_i is the charge, η_i, the electrochemical potential, and σ_i, the ionic conductivity:

$$\sigma_i = q_i c_i u_i \tag{2}$$

where c_i is the carrier concentration, and u_i, the mobility. The Nernst–Einstein equation relates the ionic mobility to the diffusion coefficient, D_i:

$$D_i = \frac{u_i kT}{q_i} \tag{3}$$

where k is the Boltzmann's constant, and T, the temperature. Using Eqs. (2) and (3), the ionic conductivity can be expressed as

$$\sigma_i = \frac{D_i q_i^2 c_i}{kT} \tag{4}$$

E-mail address: vvbelous@mail.ru.

0955-2219/$ – see front matter © 2007 Elsevier Ltd. All rights reserved.
doi:10.1016/j.jeurceramsoc.2007.01.014

Wagner's equation has phenomenological character and describes electrical and mass transport processes independent of a concrete mechanism for ion transfer. Therefore, the ionic conductivity can be measured experimentally or calculated theoretically within the framework of a microscopic theory, which is related with a choice of a concrete model for ionic transport. Three basic models[11] are used for description of the bulk ionic conduction: hopping model, stochastic model, and model of quasi-free ions. The space charge layer model[3] describes the surface ionic conduction. This model is discussed in some details below.

3. Space charge layer model

The space charge region is formed near interfaces in ionic materials to compensate charged impurities and defects, which segregate to the grain and phase boundaries. The space charge layer model for ionic materials was developed by Maier.[3] The basic concept is that ions can be trapped at the interface core. The driving force for trapping can be the existence of second phase with chemical affinity for the mobile ion. In particular, for a Frenkel-disordered ionic crystal M^+X^- (in Kröger–Vink notation[12]), the trapping of metal ions at interface sites can be written as

$$M_M + V_S \rightarrow M_S^{\cdot} + V_M' \tag{5}$$

where V_S and $M_S^{\cdot}$ are, respectively, an empty interface site and a metal ion trapped at interface site. The metal vacancies are created in the layer adjacent to the interface (space charge region). The defect profiles occur approximately within twice the Debye length (λ):

$$\lambda^2 = \varepsilon\varepsilon_0 \frac{kT}{2q^2c} \tag{6}$$

where $\varepsilon\varepsilon_0$ is the dielectric permittivity, c, the bulk defect concentration. At equilibrium, the electrochemical potential, $\eta(x)$, of charged metal vacancies is constant across the interface:

$$\eta(x) = \mu(x) + q\varphi(x) \tag{7}$$

$\mu(x)$ and $\varphi(x)$ are the local chemical and electrical potentials, respectively.

$$\mu(x) = \mu^0 + kT \ln c(x), \tag{8}$$

$c(x)$ is the local defect concentration. The equilibrium condition is:

$$\mathrm{d}\eta(x) = \mathrm{d}(kT \ln c(x) + q\varphi(x)) = 0 \tag{9}$$

The defect concentration profile in the space charge region can be expressed as

$$c(x) = c \exp\left[-q\frac{\varphi(x) - \varphi}{kT}\right] \tag{10}$$

where φ is the bulk electrical potential. The local defect concentration in the space charge region depends on the difference between the local and bulk electrical potentials. If $\varphi(x) - \varphi < 0$, the concentration of negative defects is decreased by the exponential factor while those of the positive defects is increased by the same factor and vice versa for $\varphi(x) - \varphi > 0$. Three types of space charge regions can exist: accumulation, depletion, and inversion layers.

The ionic mobility depends on several factors the most important being the height of the potential barrier that the ion must overcome to pass from one well to an adjacent well. The space charge layer model assumes that the ionic mobility in space charge region does not differ significantly from the bulk ionic mobility. In weak electrochemical field, the ionic mobility in space charge region can be written as

$$u = \left(\frac{q\gamma l^2 \nu}{kT}\right) \exp\left(-\frac{E}{kT}\right) \tag{11}$$

where ν is the hopping frequency, l, the jump distance, E, the activation energy, and γ, the geometric correction factor. According to the Eq. (2), the local ionic conductivity, $\sigma(x)$, in the space charge region can be written as

$$\sigma(x) = qc(x)u \tag{12}$$

The space charge layer model was developed for explanation of enhanced ionic conductivity in composites (heterogeneously doped systems).

4. Materials

4.1. Polycrystalline materials

The polycrystalline materials can be considered as heterogeneous, which consist of the bulk (grains) and the surface (grain boundaries) phases. The problem of the electrical current passing through heterogeneous structure was formulated firstly by Maxwell.[13] He considered specific features pertinent to the current flow in a two-phase system, which represents the condensed state. Odelevski[14] considered the arrangement of heterogeneous structures. He showed that two different arrangements are possible: matrix distributed structures, when one out of two or several composite phases (no matter how small a volume it occupies) form a continuous matrix, and statistically distributed structures. Polycrystalline materials can be classified as matrix distributed structures, as the grain boundaries form the continuous matrix. The effective conductivity of distributed structures depends on the conductivities of composed phases and their volume fractions.

The influence of grain boundaries on the electrical, diffusive and defect properties of polycrystalline materials is well known. For example, in ZnO varistors, grain boundaries with a decreased concentration of free electrons contribute to the enhancement of total resistance by ten orders of magnitude.[15,16] Similarly, the segregation of impurities such as SiO_2 at the grain boundaries in stabilized zirconia and ceria decreases the effective oxygen ion conductivity by several orders of magnitude.[17] Alternatively, grain boundaries may serve as "short circuiting pathway" in materials in which the bulk structure does not offer high ionic mobilities. This was established in the diffusion stud-

ies on NiO,[18] Al_2O_3,[19,20] ZnO,[21] and CoO.[22] In these materials, the grain boundary diffusion coefficients are by several orders of magnitude larger than the bulk diffusion coefficients at high temperature. The enhanced diffusion at the grain boundaries is related to the very large disorder of the grain boundary cores, where a high percentage of displaced atoms with corresponding strained bonds and an excess volume exist.[23] At the grain boundary core, the ionic defect formation and migration energies may be decreased. Therefore, the defect concentration and their mobility at the grain boundary core can be increased. Grain boundary cores thus intrinsically appear to possess two key characteristics necessary for enhanced ionic transport: high defect densities and high mobility. However, the high ionic transport at the grain boundary core is insufficient to ensure the high ionic transport of materials, because the fractional cross-sectional area of grain boundaries is very small in conventional polycrystalline materials. However, in nanostructured materials,[24] the fractional cross-sectional area of grain boundaries is increased considerably. Here a significant fraction of the ions (approximately 30%) lie in the disordered core of the grain boundaries and can be expected to contribute to the enhanced conductivity. An additional factor for enhanced conduction at the grain boundaries is related to the formation of the accumulation type space charge region. For a solid with $\varepsilon = 10$, $c = 10^{22}\ m^{-3}$, and $q = 2$ at 1000 K the space charge width is approximately 30 nm. Thus, the effective boundary width contributing to enhanced conductivity may be many times greater than the grain boundary core width, which is about 1 nm. Maier[3] estimates the additional boundary contribution, $\Delta\sigma_b$, to be:

$$\Delta\sigma_b = \left(\frac{4\lambda}{d}\right)(\sigma'_{sc} + \sigma''_{sc}) \tag{13}$$

where σ'_{sc} and σ''_{sc} are the mean space charge conductivities due to vacancies and interstitials, respectively, d is the average grain size. However, the boundary conductivity is proportional to both Debye length and carrier concentration. As $\lambda \sim 1/c^{1/2}$, the wider layer and the lower effective concentration are at the higher Debye length.

An additional effect on conductivity can be observed when grain size approaches the Debye length. In this case, the space charge region overlap and the defect density no longer riches the bulk value even at the center of the grain. In the limit of very small grains, local charge neutrality in nowhere satisfied and a full accumulation of charge carriers can occur with major consequences for ionic conductivity.[25–29]

In the last decade a number of nanostructured ionic conductors have been prepared and their transport properties have been reported.[30–39] For example, Puin et al.[30] have showed that the ionic conductivity in nanocrystalline CaF_2 ceramics is larger than in conventional ceramic samples. Increased electronic/ionic conductivity was observed in undoped nanocrystalline CeO_2 ceramics and thin films,[31–36] and in gadolinia-doped ceria (GDC) thin films.[37] Huang et al.[37] have showed the enhancement of ionic conductivity of nano-scale GDC thin films with thicknesses compared to grain size (20–50 nm) by several orders of magnitude in comparison with conventional polycrystalline

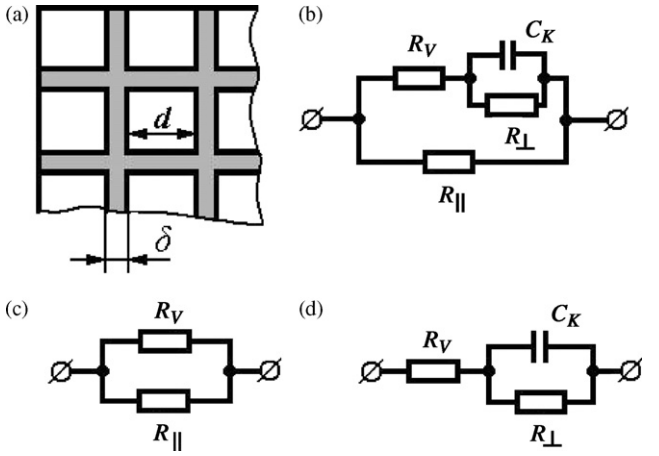

Fig. 1. Schematic of polycrystalline material (a), and its equivalent electrical circuits (b–d).

samples. Kosacki et al.[38] have prepared nanocrystalline thin films of yttria-stabilized zirconia (YSZ). Nanocrystalline YSZ thin films exhibited a two order of magnitude enhancement in ionic conductivity compared to single and conventional polycrystalline YSZ. The correct orders of magnitudes of conductivities and activation energies obtained in experiments suggest dominating surface transport.

In analyzing the effects of grain-size on conductivity, it is important to be able to comment on the relative effects of boundaries both parallel and perpendicular to the current flow. Fig. 1a shows schematically a polycrystalline material, where cubic grains with dimension d on each side are separated by grain boundaries (width of grain boundary core is δ). In general case, equivalent electrical circuit of polycrystalline material is presented in Fig. 1b, where R_v is the resistance of grains, $R_{||}$ and $R_\perp$ are the resistances of grain boundaries, respectively, lying parallel and perpendicular to the current flow, and C_k is the capacitance of intergranular contacts.[11] If the ionic conductivity in the grain boundary core, σ_s, is much higher than in the grains, σ_v, and

$$\delta\sigma_s \gg d\sigma_v \tag{14}$$

is fulfilled, we can ignore the impedance of grain boundaries laying perpendicular to the current flow. Equivalent electrical circuit for that case is presented in Fig. 1c. The opposite case is that if the ionic conductivity in the grains is much higher than in the grain boundary core, and

$$\delta\sigma_s \ll d\sigma_v \tag{15}$$

is fulfilled, than we can ignore the conduction of grain boundaries laying parallel to the current flow. The equivalent electrical circuit for that case is presented in Fig. 1d. Thus, in the first case (Fig. 1c), the grain boundaries may serve as "short circuiting pathway" for ion transport. More detailed report for the ionic conductivity and impedance of polycrystalline materials is given in Ref. 40.

4.2. Composites

The phase boundaries can substantially influence the transport properties of composites. Liang[7] observed an enhancement of ionic conductivity in the LiI/Al_2O_3 composite. The conductivity of Li^+ ions is increased by a factor of almost 50 if the LiI ceramic matrix contains Al_2O_3 fine insulator particles. Later on, conductivity enhancement effects were established for numerous ceramic composites including dispersions of fine insulator particles (Al_2O_3, SiO_2, CeO_2, B_2O_3, $BaTiO_3$ and etc.) in an ionic conductor matrix and mixtures of two different ionic conductors.[41,42]

According to the space charge layer model,[3] the ions can be trapped at the phase boundary core. Driving force is the chemical affinity of second phase to trap the ions. In particular, basic oxides present sufficiently nucleophilic hydroxide surface groups, which can attract and fix cations. $TlCl/Al_2O_3$ composite is a striking example, where a charge carrier inversion layer is observed. TlCl is an anion conductor.[3] However, in composite, Tl^+ ions are trapped and fixed at the phase boundaries with nucleophilic alumina so that thallium vacancies are enriched in the space charge region. As a result, cation conduction becomes predominant in the composite. This mechanism for conductivity enhancement is confirmed by experiments with surface-modified oxides.[3] Alumina particles treated with chlorotrimethylsilane, where the reaction:

$$\text{–OH} + (CH_3)_3\text{–SiCl} \rightarrow \text{HCl} + \text{–OSi}(CH_3)_3 \quad (16)$$

reduces the number of hydroxide surface groups. In that case, the smaller conductivity enhancement was found for $AgCl/Al_2O_3$ and AgI/Al_2O_3 composites with such surface-modified Al_2O_3. The order of oxide activity ($Al_2O_3 > SiO_2$) in composites corresponds to the pH (Al_2O_3) = 9 and pH (SiO_2) = 4 values of zero charge.[3]

Maier[3] assumed a simplified topological model of composites, and calculated their ionic conductivity. The conductivity of composites can be written as a function of the volume fraction, V_2, of the second phase with average grain size, d_2:

$$\sigma_i = (1 - v_2)\sigma + \beta\left(\frac{3v_2}{d_2}\right)(2\varepsilon\varepsilon_0\, kTc)^{1/2}u \quad (17)$$

The correction factor β has value between 0.2 and 0.7. Formula (17) is in satisfactory agreement with experiments in an intermediate range of second phase volume fraction, where a linear relation can be expected. However, a linear relation cannot be fulfilled near critical points. Two thresholds exist in "ionic conductor/insulator" composites. First, where the some part of a highly conducting continuous network in the ionic conductor matrix forms and contributes to ionic conductivity enhancement. With further increase of the second phase volume fraction, the ionic conductivity of composite is increased. The second threshold is where the insulator particles form continuous layers around of the ionic conductor grains and block all conductivity pathways. With further increase of the second phase volume fraction, the conductivity is decreased drastically. Both thresholds were taken into account in percolative model developed by Bunde et al.[43–45] The percolation concept refers to random distribution of two phases assuming also no interaction between phases and constant grain sizes. In reality surface active particles tend to percolate the grain boundaries, and with increasing content the grain size of matrix is often found to decrease accordingly in order to obtain a monolayer situation. This is the reason why the proportionality (Eq. (17)) is often a much better approach than percolation model.

A considerable enhancement of ionic conductivity was observed in heterostructures.[46–48] Maier et al.[46] have showed experimentally that the ionic conductivity of epitaxial heterostructures depends on the interface density. CaF_2/BaF_2 heterostructures with total thickness of 500 nm and different interface density (thickness of CaF_2 and BaF_2 layers are varied from 250 to 15 nm) were prepared by molecular beam epitaxy.[49] Authors have established that the heterolayered films composed of CaF_2 and BaF_2 exhibit an ionic conductivity (parallel to the interfaces) that increases proportionally with interface density. The results are in good agreement with space charge layer model, assuming a redistribution of fluoride ions at the interfaces. If the spacing is reduces further, the space charge regions overlap and size effects are observed. Similar results were presented by Peters et al.[47] for heterostructures ZrO_2/Al_2O_3. A large conductivity enhancement observed in AgI/Al_2O_3 composites has been explained by nanosized ionic heterostructures with considerable disorder in the Ag-ion sublattice.[48] Mesopore-size dependence of diffusion coefficients and ionic conductivities of LiI/mesoporous-Al_2O_3[50] and LiI/mesoporous-SiO_2[51] composites were established. These size dependences could be explained in terms of interfacial size effect.

Apart from the space charge layer and percolative models, for explanation of the enhanced ionic conductivity of composites other models were proposed. Jiang and Wagner[52] presented a model, in which the conductivity enhancement in composites is attributed to the formation of an amorphous phase at the interfaces. Belousov[5,53,54] suggested a model, in which the conductivity enhancement in composites is related to the wetting transition and formation of a highly conducting interfacial liquid phase. Let us consider this phenomenon in some details.

4.2.1. Influence of grain boundary wetting transition on transport properties of composites

Thermodynamics of wetting is a rather old branch of physics going as far back as Young's equation:

$$\gamma_{sg} = \gamma_{sl} + \gamma_{lg}\cos\theta \quad (18)$$

where θ is the contact angle; γ_{sg}, γ_{sl}, and γ_{lg} are specific free energies at the solid/gas, solid/liquid, and liquid/gas interfaces, respectively.

At the wetting transition, when $\cos\theta \rightarrow 1$, the θ angle varies around zero; hence the wetting refers to a critical phenomena. Cahn[55] demonstrated experimentally and theoretically that the wetting transition takes place in the vicinity of the critical point. He considered two-component $\alpha + \beta$ liquid brought into contact with τ solid phase. Two-phase region is confined by APCP′A′ binodal with critical point C (Fig. 2). Cahn showed that, at tem-

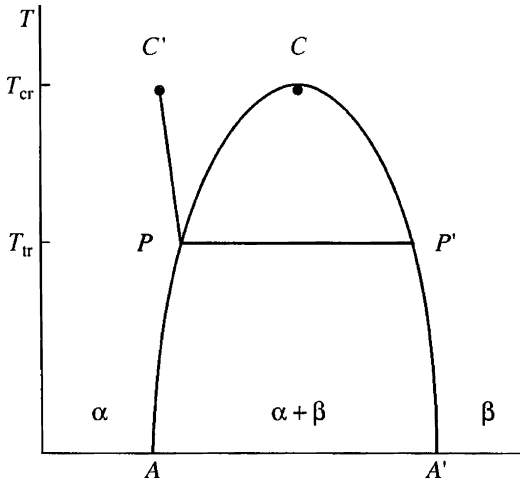

Fig. 2. Solubility diagram of binary system whose components α and β possess partial mutual solubility.

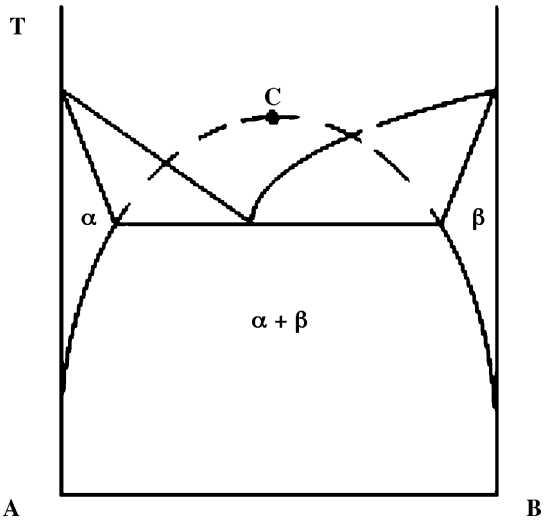

Fig. 3. Phase diagram.

perature $T \rightarrow T_{cr}$, energy $\gamma_{\alpha\beta}$ of the boundaries of α and β phases decreases faster than energy difference $\gamma_{\alpha\tau} - \gamma_{\beta\tau}$. This means that there is temperature T_{tr} above which the film of β phase exists in the two-phase area of the diagram, for example, between vessel wall τ and phase α. At temperature T_{tr}, the wetting transition is observed on the conode PP/. Cahn also showed that a thermodynamical equilibrium film of β phase can exist at the boundary between α and τ phases, as well as outside two-phase area α + β (in Fig. 2, between line PC/ and the segment of binodal PC), and called this phenomenon the prewetting transition.

Cahn's theory was repeatedly confirmed experimentally. For example, the mixture of cyclohexane and methanol has a critical point at 46 °C. Moldover and Cahn[56] experimentally demonstrated that the phase transition of cyclohexane wetting by methanol occurs when one approaches the critical temperature. In that case, a thin methanol film separates cyclohexane from the vessel wall. As the temperature lowers, reverse transition from complete to partial wetting takes place. The transition is reversible by simply increasing the temperature.

At one time there was discussion in the literature as to whether the wetting transition is a first or second order transition, i.e. whether the wetting transition is accompanied by an abrupt, discontinuous increase in thickness of the wetting phase on the surface or not. However, it is now established that the wetting transition can be both first and second order.[57]

It should also be noted that the participation of third τ phase is not required for realization of wetting transition. For example, thin film of β phase can exist at the grain boundaries of polycrystalline α phase if $\gamma_{gb} > 2\gamma_{\alpha\beta}$ (where γ_{gb} is the energy at the grain boundary of α phase). The virtual critical point *C* can be located above a solidus line in the binary phase diagram (Fig. 3). Hence, the grain boundary wetting transition can take place in the two-phase area of the bulk phase diagram, where the solid and liquid are in equilibrium.

The grain boundary wetting transition was observed for a number of ceramic composites above solidus temperature.[58–62] After the emergence of high resolution transmission electron microscopy,[63] thin intergranular amorphous films were discovered in numerous ceramic composites.[64–89] The study of microstructures demonstrated that most of wetting phase is located at the triple grain junctions.[78] The thickness of intergranular films is often constant (1–2 nm) and practically does not change from boundary to boundary. This implies that the film thickness does not depend on the angle of grain disorientation except for low-angle and special grain boundaries where intergranular films were not disclosed.

The equilibrium thickness of the intergranular wetting films in ceramic materials was estimated by Clarke.[61,90] Within the framework of continuum approximation, Clarke proposes the approach based on the balance of forces normal to the boundary:

$$P_{app} + P_{cap} + \Pi_{vdw} + \Pi_{edl} + \Pi_{str} = 0 \quad (19)$$

where P_{app} is the external pressure, P_{cap}, the capillary pressure, Π_{vdw}, the van der Waals pressure, Π_{edl}, the osmotic pressure due to the presence of any electrical double layer, and Π_{str}, the structural disjoining pressure. The thickness of intergranular wetting films thus calculated is close to that obtained in experiment. Nevertheless, much should be done to elucidate whether experimentally observed intergranular films are wetting, or prewetting, or adsorption films. Most likely these are adsorption films formed on the grain boundaries in equilibrium with the liquid phase at high temperature. Presumably, these adsorption films are left on grain boundaries after dewetting transition and retracting wetting liquid to the triple and quadruple grain junctions upon ceramics cooling. This hypothesis can be confirmed by the experimental data[81,86–88] testifying that in many ceramic composites the composition of intergranular films and second phase at the triple grain junctions differs considerably. It should also be noted that the value of the thickness of the intergranular wetting films, 1 nm, calculated by Clarke within the framework of continuum approximation is still the matter of controversy. Derjaguin et al.[91] showed that the applicability of continuum approximation is limited in the region of nanometer scales; hence, quantitative estimates are unreliable. It remains to be established whether these thin intergranular films are truly wetting, or prewetting, or adsorption films.

The grain boundary wetting transition can influence considerably transport properties of ceramic composites.[5] For example, the grain boundary wetting by eutectic melt in ceramic Bi_2CuO_4/Bi_2O_3 composite at 770 °C increases the oxygen ionic conductivity.[92] Fig. 4a presents the starting microstructure of such composite. The light phase of Bi_2O_3 is randomly distributed in the Bi_2CuO_4 matrix. Fig. 4b and c shows the microstructure of the same composite, but heated to temperature above the eutectic point between Bi_2CuO_4 and Bi_2O_3 (770 °C). In that case, Bi_2O_3 is localized at the triple grain junctions. The change of microstructure is due to a grain boundary wetting transition, which is first order.[58] Thin intergranular films were discovered in the composite cooled from temperature above eutectic point by high resolution transmission electron microscopy (Fig. 5).[5] The transition influences the ionic conductivity of composite. Fig. 6 shows an electrical conductivity of Bi_2CuO_4/Bi_2O_3 composites measured versus temperature and average grain size in air.[92,93] The curves feature jumps at 730 °C and 770 °C. The first jump is induced by the polymorphic transition of α-Bi_2O_3 to δ-Bi_2O_3.[94] The second is induced by the grain boundary wetting transition and a liquid channel grain boundary structure formation.[5,58] Both transitions are accompanied by an enhancement in the oxygen ionic conductivity.[92]

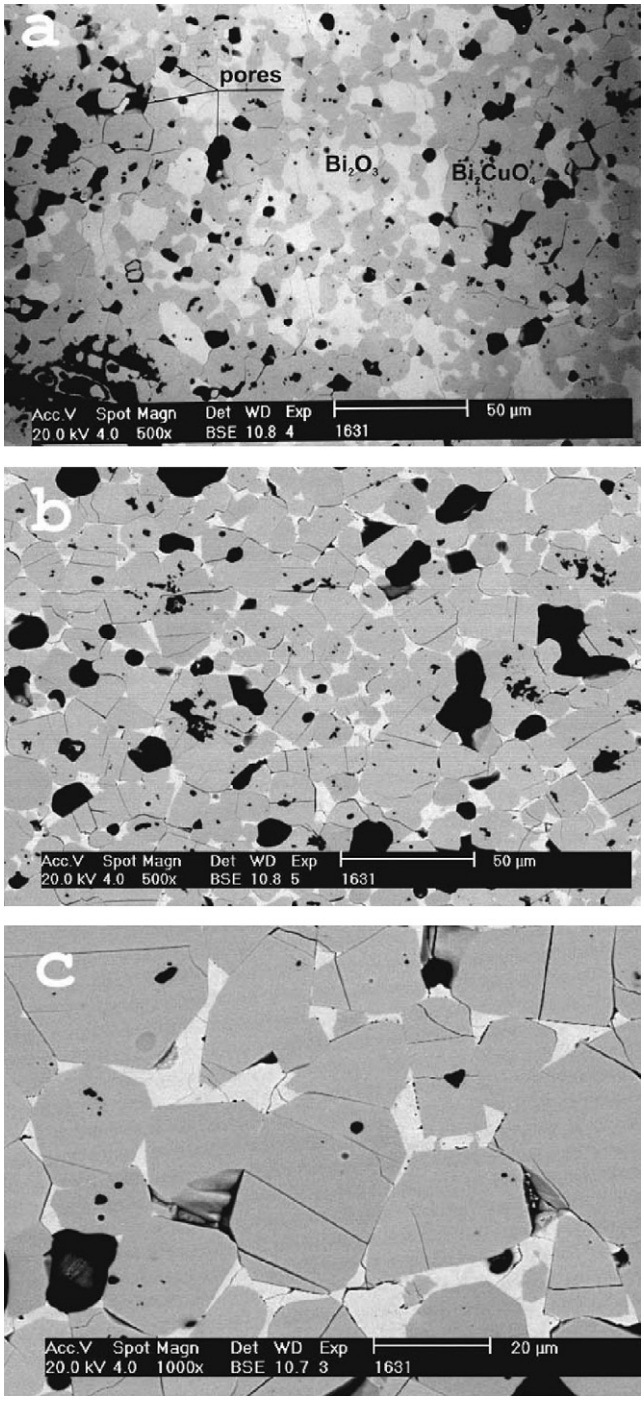

Fig. 4. Scanning electron micrograph of polished cross section of Bi_2CuO_4/Bi_2O_3 ceramic composite (a) after cooling from 700 °C, (b and c) after cooling from 780 °C: dark, light and black areas are Bi_2CuO_4, Bi_2O_3, and pores, respectively.

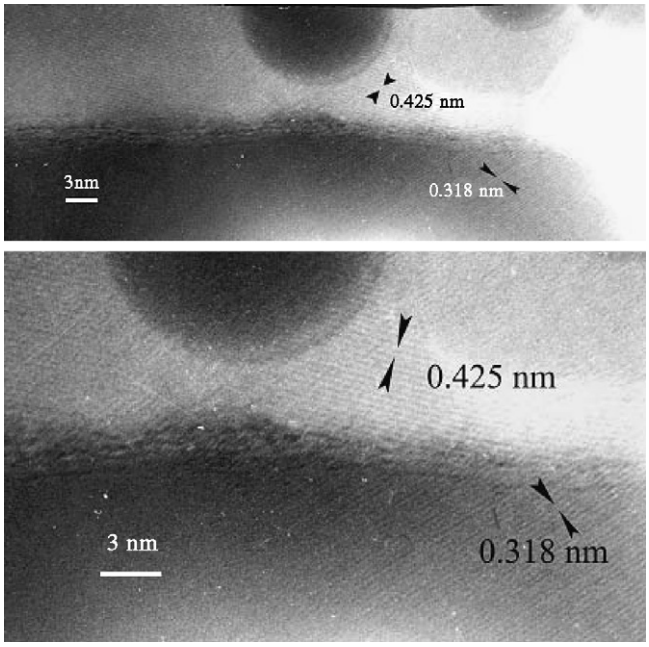

Fig. 5. High resolution transmission electron micrograph of Bi_2CuO_4/Bi_2O_3 ceramic composite after cooling from 780 °C, illustrating the existence of thin intergranular film.

The oxygen ionic conductivity and ion transference numbers of composites measured versus average grain size at 780 °C are presented in Table 1.[92] The higher ionic conductivity of composites with smaller average grain size is due to the higher density of intergranular liquid channels. These intergranular liquid channels can serve as diffusion pathways for ions as the activation energy of ion diffusion in a liquid is lower than in a solid. The intergranular liquid channels give the composite high ionic conductivity and plasticity. They can also provide capillary-osmotic, electro-kinetic and other improved mass transport properties. For example, if grain boundary wetting occurs in the protective oxide scales on metals during high temperature oxidation, the rapid mass transport along the intergranular liquid channels results in catastrophic degradation of the metal. Such a grain boundary wetting transition takes place in oxide scale containing Bi_2CuO_4 and Bi_2O_3 phases at high temperature oxidation

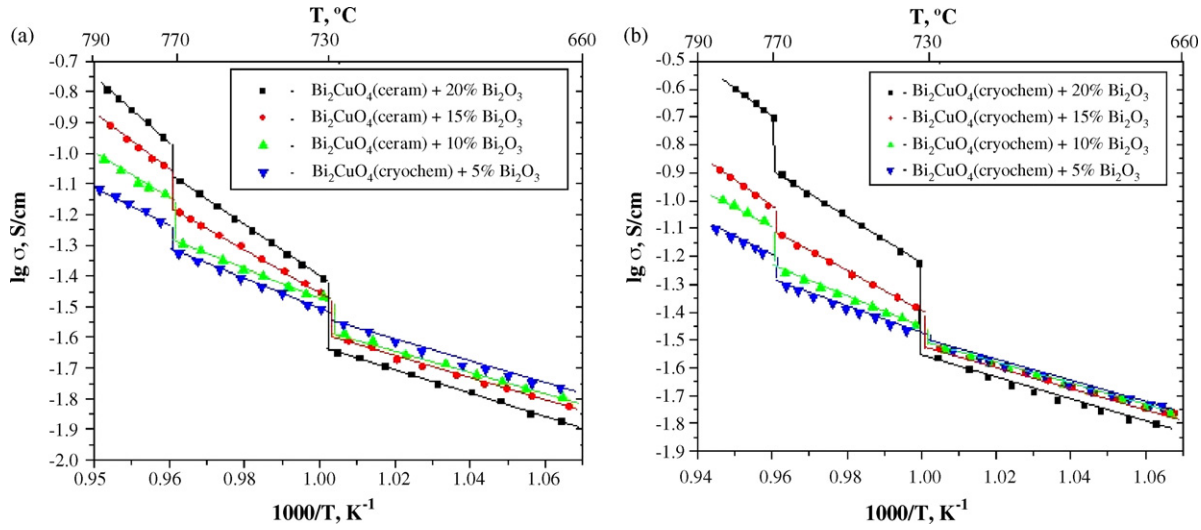

Fig. 6. Temperature dependence of electrical conductivity of $Bi_2CuO_4 + xBi_2O_3$ ($x = 5$, 10, 15, and 20 mass%) composite ceramics measured vs. average grain size (d), (a) $d = 20$ μm, and (b) $d = 10$ μm.

Table 1
Oxygen ionic conductivity (σ) and transference numbers (t_i) of Bi_2CuO_4/Bi_2O_3 composite ceramics measured vs. composition and average grain size (d) at 780 °C

Composition (mass%)	h	σ (S/m)	d (μm)
$Bi_2CuO_4 + 5\%\ Bi_2O_3$	0.02	0.12	20
$Bi_2CuO_4 + 5\%\ Bi_2O_3$	0.01	0.07	10
$Bi_2CuO_4 + 10\%\ Bi_2O_3$	0.03	0.22	20
$Bi_2Cu0_4 + 10\%\ Bi_2O_3$	0.05	0.42	10
$Bi_2CuO_4 + 15\%\ Bi_2O_3$	0.14	1.26	20
$Bi_2CuO_4 + 15\%\ Bi_2O_3$	0.18	1.68	10
$Bi_2CuO_4 + 20\%\ Bi_2O_3$	0.26	2.91	20
$Bi_2CuO_4 + 20\%\ Bi_2O_3$	0.32	6.50	10

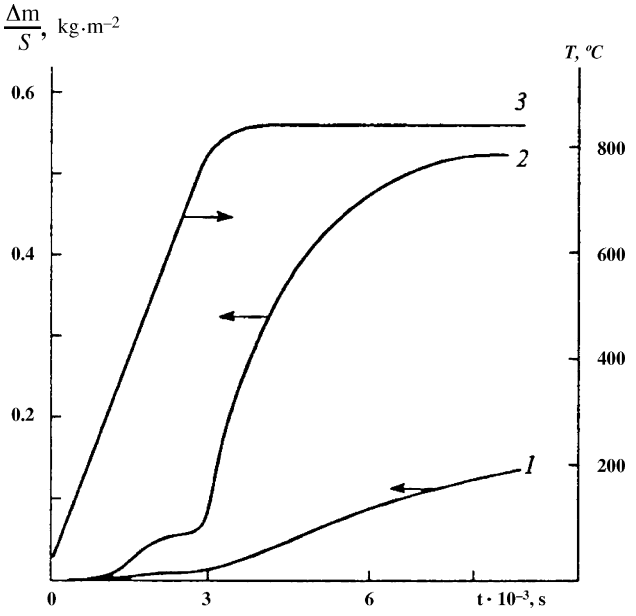

Fig. 7. Oxidation kinetics of (1) uncoated and (2) Bi-coated (30 μm) copper (20 mm × 20 mm × 0.4 mm); m is the mass, S, the copper area, T, the temperature, and t, the time.

of copper covered with thin film of bismuth.[95,96] As a result, the copper is oxidized catastrophically. Fig. 7 presents the kinetics of copper oxidation coated with a bismuth thin film (curve 2) and without coating (curve 1). Fig. 7 shows that the copper coated with a bismuth thin film is oxidized catastrophically at 770 °C. A theory of catastrophic oxidation of metals is given in Refs. 95,97

5. Concluding remarks

Interfaces play an important role in transport processes. However, the mechanisms of mass transfer at the interfaces are not adequately explored. The existent models are based on traditional concept of bulk mass transfer by point defects. Influence of surface phase transitions on transport properties of ionic conductors is investigated insufficiently. Recently, interfacial phase transitions and the formation of interfacial thin films in ionic materials are established.[5,48,62,64] Thereupon, the study of surface phase equilibrium and the construction of surface phase diagrams will open broad opportunities in the control of transport properties of ionic materials.

References

1. Kiselev, V. F., Kozlov, S. N. and Zoteev, A. V., *Fundamentals of Surface Physics of Solids*. MSU, Moscow, 1999.
2. Maier, J., *Physical Chemistry of Ionic Materials*. Wiley, Chichester, 2004.
3. Maier, J., Ionic conduction in space charge regions. *Prog. Solid St. Chem.*, 1995, **23**, 171–263.
4. Maier, J., Point-defect thermodynamics and size effects. *Solid State Ionics*, 2000, **131**, 13–22.
5. Belousov, V. V., Grain boundary wetting in ceramic cuprates. *J. Mater. Sci.*, 2005, **40**, 2361–2365.
6. Knauth, P. and Tuller, H. L., Solid state ionics: roots, status, and future prospects. *J. Am. Ceram. Soc.*, 2002, **85**, 1654–1680.
7. Liang, C. C., Conduction characteristics of the lithium iodide-aluminum oxide solid electrolytes. *J. Electrochem. Soc.*, 1973, **120**, 1289–1292.
8. Schoonman, J., Nanostructured materials in solid state ionics. *Solid State Ionics*, 2000, **135**, 5–19.

9. Wagner, J. B., Composite solid ion conductors. In *High Conductivity Solid Ionic Conductors*, ed. T. Takahashi. World Scientific, Singapore, 1989, pp. 146–165.
10. Wagner, C., *Z. Phys. Chem. (Leipzig)*, 1936, **32**, 447.
11. Chebotin, V. N. and Perfil'ev, M. V., *Electrochemistry of Solid Electrolytes*. Chemistry, Moscow, 1978.
12. Kroger, F. A., ed., *The Chemistry of Imperfect Crystals*. 2nd ed. Amsterdam, North-Holland, 1974.
13. Maxwell, J. C., *A Treatise on Electricity and Magnetism*, *vol. 1*. Clarendon, Oxford, 1881, p. 403.
14. Odelevski, V. I., Calculation of the generalized conductivity of heterogeneous systems. *Zh. Tekh. Fiz.*, 1951, **21**, 661–675.
15. Gupta, T. K., Applications of zinc oxide varistors. *J. Am. Ceram. Soc.*, 1990, **73**, 1817–1840.
16. Clarke, D. R., Varistor ceramics. *J. Am. Ceram. Soc.*, 1999, **82**, 485–502.
17. Badwal, S. P. S. and Rajendran, S., Effect of microstructure and nanostructure on the properties of ionic conductors. *Solid State Ionics*, 1994, **70–71**, 83–95.
18. Atkinson, A., Surface and interface mass transport in ionic materials. *Solid State Ionics*, 1988, **28–30**, 1377–1387.
19. Oishi, Y. and Kingery, W. D., Oxygen diffusion in periclose crystals. *J. Phys. Chem.*, 1960, **33**, 905–906.
20. Moya, E. G., In *Science of Materials Interfaces*, ed. J. Nowotny. Elsevier, Amsterdam, 1993.
21. Tuller, H. L., ZnO Grain boundaries: electrical activity and diffusion. *J. Electroceram.*, 1999, **4**, 33–40.
22. Kowalski, K., Moya, E. G. and Nowotny, J., Grain boundary diffusion in CoO. *J. Phys. Chem. Solids*, 1996, **57**, 153–163.
23. Kalinin, S. V., Shao, R. and Bonnell, D. A., Local phenomena in oxides by advanced scanning probe microscopy. *J. Am. Ceram. Soc.*, 2005, **88**, 1077–1098.
24. Gleiter, H., Nanostructured materials: basic concepts and microstructure. *Acta Mater.*, 2000, **48**, 1–29.
25. Maier, J., Space charge regions in solid two phase systems and their conduction contribution – III: defect chemistry and ionic conductivity in thin films. *Solid State Ionics*, 1987, **23**, 59–67.
26. Maier, J., Thermodynamics aspects and morphology of nano-structured ion conductors. Aspects of nano-ionics. Part I. *Solid State Ionics*, 2002, **154–155**, 291–301.
27. Maier, J., Defect chemistry and ion transport in nanostructured materials. Part II. Aspects of nanoionics. *Solid State Ionics*, 2003, **157**, 327–334.
28. Maier, J., Nano-sized mixed conductors (aspects of nano-ionics. Part III). *Solid State Ionics*, 2002, **148**, 367–374.
29. Maier, J., Ionic transport in nano-sized systems. *Solid State Ionics*, 2004, **175**, 7–12.
30. Puin, W., Rodewald, S., Ramlau, R., Heitjans, P. and Maier, J., Local and overall ionic conductivity in nanocrystalline CaF_2. *Solid State Ionics*, 2000, **131**, 159–164.
31. Chang, Y. M., Lavik, E. B., Kosacki, I., Tuller, H. L. and Ying, J. V., Nonstoichiometry and electrical conductivity of nanocrystalline CeO_{2-x}. *J Electroceram*, 1997, **1**, 7–14.
32. Kosacki, I. and Anderson, H. U., *Encyclopedia of Materials Science and Technology*, *Vol. 4*. Elsevier Science, New York, 2000, p. 3609.
33. Suzuki, T., Kosacki and Anderson, H. U., Defect and mixed conductivity in nanocrystalline doped cerium oxide. *J. Am. Ceram. Soc.*, 2002, **85**, 1492–1498.
34. Aoki, M., Chang, Y. M., Kosacki, I., Lee, J. R., Tuller, H. L. and Lin, Y. J., Solute segregation and grain boundary impedance in high-purity stabilized zirconia. *J. Am. Ceram. Soc.*, 1996, **79**, 1169–1180.
35. Mondal, P., Klein, A., Jagermann, W. and Hahn, H., Enhanced specific grain boundary conductivity in nanocrystalline Y_2O_3-stabilized zirconia. *Solid State Ionics*, 1999, **118**, 331–339.
36. Tchope, A., Grain-size dependent electrical conductivity of polycrystalline cerium oxide II: space charge model. *Solid State Ionics*, 2001, **139**, 267–280.
37. Huang, H., Gur, T. M., Saito, Y. and Prinz, F., *Ultra thin gadolinia-doped ceria (GDC) films: ionic conduction characteristics and application in SOFC*. Book of Abstract, SSI-15, Baden-Baden, 2005, p. 83, July 17–22.
38. Kosacki, I., Gorman, B. and Anderson, H. U., *Ionic and Mixed Conductors*, *vol. 3*, ed. T. A. Ramanarajanan. Electrochemical Society, Pennington, NJ, 1998, p. 631.
39. Tuller, H. L., Ionic conduction in nanocrystalline materials. *Solid State Ionics*, 2000, **131**, 143–157.
40. Maier, J., On the conductivity of polycrystalline materials. *Ber. Bunsenges. Phys. Chem.*, 1986, **90**, 26–33.
41. Agrawal, R. C. and Gupta, R. K., Superionic solids: composite electrolyte phase—an overview. *J. Mater. Sci.*, 1999, **34**, 1131–1162.
42. Knauth, P., Ionic conductor composites: theory and materials. *J. Electroceram.*, 2000, **5**, 111–125.
43. Bunde, A., Dieterich, W. and Roman, E., Monte-carlo studies of ionic conductors containing an insulating second phase. *Solid State Ionics*, 1986, **18–19**, 147–150.
44. Indris, S., Heitjans, P., Roman, H. E. and Bunde, A., Nanocrystalline versus microcrystalline $Li_2O{:}B_2O_3$ composites: anomalous ionic conductivities and percolation theory. *Phys. Rev. Lett.*, 2000, **84**, 2889–2892.
45. Knauth, P., Albinet, G. and Debierre, J. M., Electrical conductivity of model composites of an ionic conductor (CuBr) and an insulator (TiO_2, Al_2O_3): experiments and percolation – type model. *Solid State Ionics*, 1999, **121**, 101–106.
46. Sata, N., Eberman, K., Eberl, K. and Maier, J., Mesoscopic fast ion conduction in nanometer-scale planar heterostructures. *Nature (London)*, 2000, **408**, 946–948.
47. Peters, A., Korte, C., Hesse, D. and Janek, J., *Ionic conduction in zirconia/alumina hetero-multilayers*. Book Abstract, SSI-15, Baden-Baden, 2005, p. 186, July 17–22.
48. Lee, J. S., Adams, S. and Maier, J., A mesoscopic heterostructure as the origin of the extreme ionic conductivity in $AgI{:}Al_2O_3$. *Solid State Ionics*, 2000, **136–137**, 1261–1266.
49. Eberl, K., Petroff, P. M. and Demeester, D., ed., *Proceedings of the NATO Advanced Research Workshop*. Kluwer, Dordrecht, 1995.
50. Maekawa, H., Shen, H., Fujimaki, Y., Kawata, K. and Yamamura, T., *Mesopore size dependence of ionic conductivity of alumina based composite*. Book Abstract, SSI-15, Baden-Baden, 2005, p. 23, July 17–22.
51. Yamada, H., Moriguchi, I. and Kudo, T., Nano-structured Li-ionic conductive composite solid electrolyte synthesized by using mesoporous SiO_2. *Solid State Ionics*, 2005, **176**, 945–953.
52. Jiang, S. and Wagner, J. B., J. Theoretical model for composite electrolytes. I. Space charge layer as a cause for carrier enhancement. *Phys. Chem. Solids*, 1995, **56**, 1101–1111.
53. Belousov, V. V., Liquid channel grain boundary structures. *J. Am. Ceram. Soc.*, 1996, **79**, 1703–1706.
54. Belousov, V. V., Liquid-channel grain-boundary structures with ionic conduction. *Russ. J. Electrochem.*, 1995, **31**, 1240–1244.
55. Cahn, J. W., Critical point wetting. *J. Chem. Phys.*, 1977, **66**, 3667–3672.
56. Moldover, M. R. and Cahn, J. W., Interface phase transition—complete to partial wetting. *Science*, 1980, **207**, 1073–1075.
57. Teletzke, G. F., Scriven, L. E. and Davis, H. T., Wetting transitions: first order or second order? *J. Chem. Phys.*, 1982, **77**, 5794–5798.
58. Belousov, V. V., Wetting of grain boundaries in ceramic materials. *Colloid J.*, 2004, **66**, 121–127.
59. Belousov, V. V., Rapid nondiffusional penetration of oxide melts along grain boundaries of oxide ceramics. *J. Am. Ceram. Soc.*, 1999, **82**, 1342–1344.
60. Belousov, V. V., Surface energy of bismuth cuprate. *J. Supercond.*, 2002, **15**, 207–210.
61. Clarke, D. R. and Gee, M. L., Wetting of surfaces and grain boundaries. In *Materials Interfaces*, ed. D. Wolf and S. Yip. Chapman and Hall, London, 1992, pp. 255–272.
62. French, R. H., Origins and applications of London dispersion forces and Hamaker constants in ceramics. *J. Am. Ceram. Soc.*, 2000, **83**, 2117–2146.
63. Newbury, D. E. and Williams, D. B., The electron microscope: the materials characterization tool of the millennium. *Acta Mater.*, 2000, **48**, 323–346.
64. Juo, J. and Chiang, Y. M., Existence and stability of nanometer-thick disordered films on oxide surfaces. *Acta Mater.*, 2000, **48**, 4501–4515.
65. Callahan, D. L. and Thomas, G., Impurity distribution in polycrystalline aluminum nitride ceramics. *J. Am. Ceram. Soc.*, 1990, **73**, 2167–2170.

66. Kleebe, H. J., Cinibulk, M. K., Cannon, R. M. and Ruhle, M., Statistical analysis of the intergranular film thickness in silicon nitride ceramics. *J. Am. Ceram. Soc.*, 1993, **76**, 1969–1977.
67. Padture, N. P., In situ-toughened silicon carbide. *J. Am. Ceram. Soc.*, 1994, **77**, 519–523.
68. Knowles, K. M. and Turan, S., The dependence of equilibrium film thickness on grain orientation at interface boundaries in ceramics-ceramics composites. *Ultramicroscopy*, 2000, **83**, 245–259.
69. Tanaka, L., Kleebe, H. J., Cinibulk, M. K., Bruley, J., Clarke, D. R. and Ruhle, M., Calcium concentration dependence of the intergranular film thickness in silicon nitride. *J. Am. Ceram. Soc.*, 1994, **77**, 911–914.
70. Wang, C. M., Pan, X., Hoffman, M. J., Cannon, R. M. and Ruhle, M., Grain boundary films in rare-earth-glass-based silicon nitride. *J. Am. Ceram. Soc.*, 1996, **79**, 788–792.
71. Clarke, D. R., Grain boundaries in polycrystalline ceramics. *Ann. Rev. Mater. Sci.*, 1987, **17**, 57–74.
72. Shaw, T. M. and Duncombe, P. R., Forces between aluminum oxide grains in a silicate melt and their effect on grain boundary wetting. *J. Am. Ceram. Soc.*, 1991, **74**, 2495–2505.
73. Wiederhorn, S. M., Hockey, B. J. and French, J. D., Mechanisms of deformation of silicon nitride and silicon carbide at high temperature. *J. Eur. Ceram. Soc.*, 1999, **19**, 2273–2284.
74. Susnitzky, D. W. and Carter, C. B., Structure of alumina grain boundaries prepared with and without a thin amorphous intergranular films. *J. Am. Ceram. Soc.*, 1990, **73**, 2485–2493.
75. Powelt-Dogan, C. A. and Heuer, A. H., Microstructure of 96% alumina ceramics: I, characterization of the as-sintered materials. *J. Am. Ceram. Soc.*, 1990, **73**, 3670–3676.
76. Kim, D. Y., Wiederhorn, S. M., Hockey, B. J., Blendell, J. E. and Handwerker, C. A., Stability and surface energy of wetted grain boundaries in aluminum oxide. *J. Am. Ceram. Soc.*, 1994, **77**, 444–453.
77. Blendell, J. F., Carter, W. C. and Handwerker, C. A., Faceting and wetting transitions of anisotropic interfaces and grain boundaries. *J. Am. Ceram. Soc.*, 1999, **82**, 1889–1900.
78. Lee, J. R., Chiang, Y. M. and Ceder, G., Pressure-thermodynamic study of grain boundaries: Bi segregation in ZnO. *Acta Mater.*, 1997, **45**, 1247–1257.
79. Ernst, F., Kienzle, O. and Ruhle, M., Structure and composition of grain boundaries in ceramics. *J. Eur. Ceram. Soc.*, 1997, **19**, 665–673.
80. Ramamurty, S., Mallamaci, M. P., Zimmerman, C. M., Carter, C. B., Duncombe, P. R. and Shaw, T. M., Microstructure of polycrystalline MgO penetrated by a silicate liquid. *JMSA ISSN*, 1996, **2**, 113–128.
81. Brydson, R., Chen, S. C., Riley, F. L., Milne, S. J., Pan, X. and Ruhle, M., Microstructure and chemistry of intergranular glassy films in liquid-phase-sintered alumina. *J. Am. Ceram. Soc.*, 1998, **81**, 369–379.
82. Gu, H., Cannon, R. M. and Ruhle, M., Composition and chemical width of ultra-thin intergranular amorphous film in silicon nitride. *J. Mater. Res.*, 1998, **13**, 476–487.
83. Luo, J. and Chiang, Y. M., Equilibrium thickness amorphous film on (1 1 2 0) surfaces of Bi_2O_3-doped ZnO. *J. Eur. Ceram. Soc.*, 1999, **19**, 697–701.
84. Kleebe, H. J., Structure and chemistry of interfaces in Si_3N_4 materials studied by transmission electron microscopy. *J. Ceram. Soc. Jpn.*, 1997, **105**, 453–475.
85. Gu, H., Pan, X., Cannon, R. M. and Ruhle, M., Dopant distribution in grain-boundary films in calcia-doped silicon nitride ceramics. *J. Am. Ceram. Soc.*, 1998, **81**, 3125–3135.
86. Wang, H. and Chiang, Y. M., Thermodynamic stability of intergranular amorphous filmsin Bi-doped ZnO. *J. Am. Ceram. Soc.*, 1998, **81**, 89–96.
87. Chiang, Y. M., Wang, H. and Lee, J. R., HREM and STEM of intergranular films at zinc oxide varistor grain boundaries. *J. Microsc.*, 1998, **191**, 275–285.
88. Luo, J., Wang, H. and Chiang, Y. M., Origin of solid-state activated sintering in ZnO-Bi_2O_3. *J. Am. Ceram. Soc.*, 1999, **82**, 916–920.
89. Tanaka, T., Adachi, H., Nakayasu, T. and Yamada, T., In *Ceramic Microstructure: Control at the Atomic Level*, ed. A. P. Tomsia. Plenum Press, New York, 1998.
90. Clarke, D. R., On the equilibrium thickness of intergranular glass phases in ceramic materials. *J. Am. Ceram. Soc.*, 1987, **70**, 15–22.
91. Derjaguin, B. V., Churaev, N. V. and Muller, V. M., *Surface Forces*. Science, Moscow, 1985.
92. Lyskov, N. V., Metlin, Yu. G., Belousov, V. V. and Tret'yakov, Yu. D., Electrical conductivity of Bi_2CuO_4-Bi_2O_3 ceramic composites. *Doklady Chem.*, 2003, **392**, 229–232.
93. Lyskov, N. V., Metlin, Yu. G., Belousov, V. V. and Tret'yakov, Yu. D., Transport properties of Bi_2CuO_4-Bi_2O_3 ceramic composites. *Solid State Ionics*, 2004, **166**, 207–212.
94. Harwig, H. A. and Gerards, A. G., Electrical properties of α, β, γ, and δ phases of bismuth sequioxide. *J. Solid St. Chem.*, 1978, **26**, 265–274.
95. Belousov, V. V., Catastrophic oxidation of metals. *Russ. Chem. Rev.*, 1998, **67**, 563–571.
96. Belousov, V. V., The kinetics and mechanism of catastrophic oxidation of metals. *Oxid. Met.*, 1994, **42**, 511–528.
97. Belousov, V. V. Mechanisms of copper accelerated oxidation in the presence of molten oxides. *Oxid. Met.*, in press.